Linear stability analysis of bubble-induced convection in a horizontal liquid layer

Kotaro Nakamura [1,*], Harunori N. Yoshikawa [2], Yuji Tasaka [1], and Yuichi Murai [1]

[1]*Laboratory for Flow Control, Hokkaido University, Sapporo, Japan*
[2]*Université Côte d'Azur, CNRS, Institut de Physique de Nice, 06100 Nice, France*

We investigate with a linear analysis the stability of a horizontal liquid layer subjected to injection of gas bubbles through a bottom wall. The injection is assumed uniform in space and constant in time. Injected bubbles ascend in the liquid layer due to the Archimedean buoyancy force and are ejected from the top free surface of the liquid layer. Modeling this two-phase flow system as two interpenetrating liquid and gas continua, we show that homogeneous upward gas flows become unstable at large gas fluxes. We determine the critical conditions of this homogeneous-heterogeneous regime transition and show that the critical modes are made of stationary convection rolls, either multi- or whole-layered depending on liquid viscosity, the radius of bubbles, and the thickness of liquid layer. By examining the energy transfer from base to perturbation flows, we indicate that liquid convective motion is driven by the buoyancy on heterogeneously distributed bubbles. We also reveal that the lift forces on bubbles have significant stabilizing effects by homogenizing bubble distribution close to the bottom wall.

I. INTRODUCTION

Bubbly two-phase flows have attracted much attention in various fields of scientific research because of their importance in industrial applications and because of interest in complex multiscale flow phenomena [1]. The flows occur in a large variety of applications, e.g., frictional drag reduction of naval vessels [2,3], ultrasound contrast agents [4], and efficient delivery system of drugs and genes [5].

Bubble column reactors are widely used in chemical and biological engineering processes as an efficient gas-liquid contactor for mass and heat transfer [6,7]. Bubbles injected to liquids ascend due to Archemedian buoyancy forces, exchanging mass and heat at liquid-gas interfaces. Depending on the bubble size, the flow rate of gas injection, and the geometrical shape of the reactor [8–10], the system exhibits a variety of flow patterns resulting from multiscale phenomena embedded in the dynamics of dispersed two-phase systems. When the gas flux is small, bubbles can rise in liquid with a uniform spatial distribution [8,11]. Flows in this homogeneous regime are destabilized at large gas flux and become heterogeneous, where the bubble distribution is no longer uniform. The transition from homogeneous to heterogeneous regimes is accompanied by convective motion in the liquid phase of a length scale comparable with the system size. This large-scale convection is crucial for the design of reactors [12]. Theoretical and numerical investigations on the generation of large-scale convections have been performed for semibatch and continuous operation conditions of reactors [12–14]. Different instabilities associated with the pressure

drop in gas injector arrays [12] and with lift forces on bubbles [13] are reported.

Convection in bubbly flows has also been investigated from the viewpoint of stability of fluid systems with inverse density profiles [15–17]. When a lower zone of a two-phase layer is richer in bubbles than in the upper zone, the layer is overturned by gravity-driven instabilities similar to the Rayleigh-Taylor (RT) instability. The threshold of the gravity-driven instabilities of bubble layers is often given as a Rayleigh number Ra based on the Archimedean buoyancy of the gas-dispersed liquid phase. Experiments on a RT-like instability of bubble layers show the formation of bubble plumes. For Ra $\gtrsim 2.5 \times 10^5$, steady counter-rotating convection rolls were observed by Kimura [15] and Iga and Kimura [16] (hereafter referred to as IK07). A direct numerical simulation based on a point bubble model was performed by Climent and Magnaudet [17] (hereafter referred to as CM99) for flows developing from a particular two-layer state, in which a pure liquid layer is superposed on a bubble layer. The results confirm the formation of convection rolls for Ra $\sim 2.0 \times 10^5$. The point bubble model is based on an Euler-Lagrange approach. Bubbles are regarded as point sources of buoyancy subjected to drag and lift forces. A spatially filtered Navier-Stokes equation is coupled with the equations of motion for individual point bubbles. This model does not take into account diffusion-like processes (*hydrodynamic diffusion*) in the bubble dynamics, which prevents the formation of highly buoyant bubble clusters [18] and results from direct hydrodynamic bubble-bubble interactions [19]. The results of CM99 suggest that no wave number selection exists for convection roll formation.

Ruzicka and Thomas [18] discuss the analogy between the homogeneous-heterogeneous regime transition of bubbly flows and the Rayleigh-Bénard (RB) instability. The authors

---
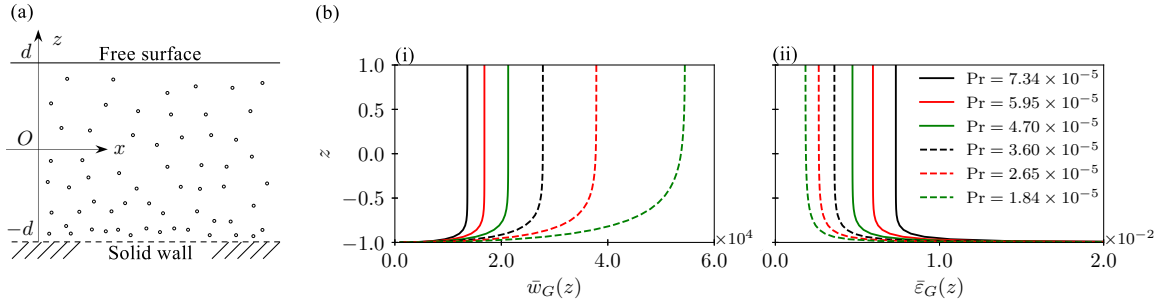
*nakamura@ring-me.eng.hokudai.ac.jp

FIG. 1. (a) Schematic illustration of the problem, and (b) (i) profiles of bubble ascending velocity $\bar{w}_G(z)$ and (ii) gas volume fraction $\bar{\varepsilon}_G(z)$ in the base state with different Pr defined as Eq. (19): the gas injection velocities and gas injection volume fractions at $z = -1$ of the profiles equal to $w_{G,0} = 1000$ and $\varepsilon_{G,0} = 0.02$, respectively.

consider rising bubbles distributed uniformly in a quiescent liquid layer, assuming hydrodynamic diffusion in the behavior of bubble swarms. They examine the analogy in detail and deduce Ra, Prandtl number Pr, and Nusselt number Nu characterizing bubble convections. Ruzicka and Thomas [18] estimate the critical value of Ra to be about 10^5 due to their experiments [20]. Though the consideration of the buoyancy-driven instability by Ruzicka and Thomas [18] remains qualitative, the analogy indicates the existence of a wave number selection mechanism. This contradicts the results of the afore-mentioned simulation (CM99) of bubbly flows [17]. This discrepancy might be explained *either* from the difference in the base states considered in these studies *or* from the effects of hydrodynamic diffusion, which are absent in CM99 [17].

In the present paper, we revisit the problem of homogeneous-heterogeneous regime transition to examine the wave number selection mechanism in the linear stage of transition by performing a linear stability analysis for ascending bubbles in a quiescent liquid layer. In contrast to the existing works on bubble column reactors [12–14], we focus on the transition provoked by the inherent dynamics of bubbly flows without any effect of gas injection systems and of lateral walls. The analysis is based on an Euler-Euler approach by a spatially filtered Navier-Stokes equation for the liquid phase coupled with an Eulerian momentum equation for bubbles. In contrast to the Euler-Euler approach of Ruzicka and Thomas [18], no hydrodynamic diffusion is taken into account. The present work would thus determine whether the hydrodynamic diffusion is essential in the wave number selection of bubble-induced convection rolls. For simplicity, only the added-mass, drag, lift, and buoyancy forces are considered in the momentum exchanges between gas and liquid phases as in CM99 [17].

The model for bubbly flows is given in Sec. II. We summarize the governing equations (Sec. II A) and apply them to a homogeneous flows of bubble rising in a quiescent horizontal liquid layer (Sec. II B). The Rayleigh and Prandtl numbers and two other numbers characterizing the bubble layer are introduced in Sec. II C with dimensionless versions of the governing equations. The linear stability problem of the homogeneous state is formulated in Sec. III. Results of the analysis are presented in Sec. IV and discussed in Sec. V. Section VI is concerned with summary.

II. THEORETICAL MODEL

A. Governing equations

We consider two-dimensional bubbly flows in a horizontal liquid layer generated by uniform injection of monodisperse spherical bubbles from the bottom wall [Fig. 1(a)]. Bubbles rise in the layer due to Archimedean buoyancy forces and are ejected from the top free surface. The velocity $W_{G,0}$ and flux $J_{G,0}$ of gas injection are maintained at constant values. We model the dynamics of this immiscible two-phase flow system using the Euler-Euler approach, in which the liquid and gas phases are regarded as two dynamical continua exchanging momentum and energy with each other. The model consists of the following mass and momentum conservation equations for gas and liquid phases:

$$\frac{\partial \varepsilon_G}{\partial t} + \boldsymbol{\nabla} \cdot (\varepsilon_G \mathbf{u}_G) = 0, \tag{1}$$

$$C_A \frac{D\mathbf{u}_G}{Dt} = (1 + C_A)\frac{D\mathbf{u}}{Dt} - \frac{3}{8R_b}C_D \|\mathbf{u}_G - \mathbf{u}\|(\mathbf{u}_G - \mathbf{u})$$
$$- C_L(\mathbf{u}_G - \mathbf{u}) \times (\boldsymbol{\nabla} \times \mathbf{u}) - \mathbf{g}, \tag{2}$$

$$\boldsymbol{\nabla} \cdot \mathbf{u} = 0, \tag{3}$$

$$\frac{D\mathbf{u}}{Dt} = -\frac{1}{\rho}\boldsymbol{\nabla}p + \nu\Delta\mathbf{u} + \mathbf{g} + \varepsilon_G\left(\frac{D\mathbf{u}}{Dt} - \mathbf{g}\right), \tag{4}$$

where ε_G is gas volume fraction, $\mathbf{u}_G = (u_G, w_G)$ and $\mathbf{u} = (u, w)$ are the velocity fields of gas and liquid, respectively, and p is the pressure field. The bubble radius, density, and kinematic viscosity of liquid and gravitational acceleration are denoted by R_b, ρ, ν, and $\boldsymbol{g}$, respectively. The differential operator D/Dt stands for the material derivative, i.e., $D\mathbf{u}_G/Dt = \partial_t\mathbf{u}_G + \mathbf{u}_G \cdot \boldsymbol{\nabla}\mathbf{u}_G$ and $D\mathbf{u}/Dt = \partial_t\mathbf{u} + \mathbf{u} \cdot \boldsymbol{\nabla}\mathbf{u}$.

In the gas momentum equation [Eq. (2)], the effects of bubble-bubble interactions inducing bubble clustering and hydrodynamic diffusion have been omitted, assuming dilute bubbly flows. We have supposed spherical nondeformable bubbles, assuming the Galilei number $\text{Ga} = \sqrt{gR_b}R_b/\nu$ and Eötvös number $\text{Eo} = \rho g R_b^2/\gamma$ are sufficiently small: $\text{Ga} \lesssim 10^2$, $\text{Eo} \lesssim 10^{-1}$ [21,22]. These hypotheses are satisfied, e.g., for bubbles of $R_b \sim 0.5$mm in water at room temperature. The first to third terms on the right-hand side of Eq. (2) arise from the momentum exchange with liquid phase. These terms

represent the effects of liquid inertia, drag, and shear-induced lift on bubble motion, respectively. The added-mass and lift coefficients, C_A and C_L, are assumed constant and given by $1/2$, supposing small bubbles [23]. For simplicity, the drag coefficient is modeled by

$$C_D = \frac{48}{\text{Re}_b}, \quad \text{with } \text{Re}_b = \frac{2R_b \|\mathbf{u}_G - \mathbf{u}\|}{\nu}, \tag{5}$$

where Re_b is the bubble Reynolds number (for the effects of the C_D model, see Appendix A). This drag model has been obtained by computing the viscous energy dissipation around a spherical bubble in a steady potential flow [24]. The bubble Reynolds number is of $O(10^2)$ for bubbles of $R_b \sim 0.5$mm ascending in water at room temperature with the terminal velocity.

In the liquid mass conservation (3) and the liquid momentum (4), we have assumed dilute bubbly flows and considered liquid flows effectively incompressible. We have also restricted our attention to flows at scales larger than the mean distance between bubbles. Bubbles affect the dynamics of the liquid phase only through the mesoscale cumulative reaction force, $\varepsilon_G D\mathbf{u}/Dt$, and buoyancy force, $-\varepsilon_G \mathbf{g}$ [25]. The same equation has been used in a Lagrangian analysis of the influence of bubbles on a carrier phase [26] and in an investigation on the liquid-gas interfacial coupling in a free-shear flow of a dilute bubble suspension [27]. Mazzitelli *et al.* [28] and Oresta *et al.* [29] model, respectively, bubble-laden isotropic turbulent flows and RB convection with vapor bubbles as the same momentum equation as Eq. (4), though the reaction from bubbles and buoyancy forces are coupled with the motions of point bubbles determined in a Lagrangian approach.

The upper surface of the liquid layer is assumed as flat and shear free for simplicity. At the bottom wall, no-slip conditions on the liquid velocity, constant gas velocity, and constant gas flux are imposed,

$$\frac{\partial u}{\partial z} + \frac{\partial w}{\partial x} = 0, \ w = 0, \quad \text{at } z = d, \tag{6}$$

$$\mathbf{u} = 0, \ w_G = W_{G,0}, \ \varepsilon_G W_{G,0} = J_{G,0}, \quad \text{at } z = -d. \tag{7}$$

B. Base state

Two-dimensional flows would respect the translational symmetry of the system along the x direction when the flux of gas injection is small. We thus assume a steady bubbly flow in the homogeneous regime, where the flow fields are laterally uniform:

$$\mathbf{u} = 0, \quad \mathbf{u}_G = \bar{w}_G(z)\, \mathbf{e}_z, \quad \varepsilon_G = \bar{\varepsilon}_G(z). \tag{8}$$

The unit vector in the z direction is denoted as $\mathbf{e}_z$. For these fields, Eqs. (1) and (2) read

$$\frac{d}{dz}(\bar{\varepsilon}_G \bar{w}_G) = 0, \tag{9}$$

$$\bar{w}_G \frac{d\bar{w}_G}{dz} = -\frac{18\nu \bar{w}_G}{R_b^2} + 2g. \tag{10}$$

We have invoked Eq. (5) for the drag force. The boundary conditions (7) read

$$\bar{w}_G = W_{G,0}, \quad \bar{\varepsilon}_G \bar{w}_G = J_{G,0}, \quad \text{at } z = -d. \tag{11}$$

The momentum equation (10) indicates that the gas phase is accelerated toward the terminal velocity $V_\infty = gR_b^2/9\nu$. Some profiles of velocity $\bar{w}_G$ calculated from Eq. (10) are shown in Fig. 1(b)(i). The gas velocity increases in a sublayer attached to the wall. Outside this sublayer the gas flows at a constant velocity V_∞.

According to Eqs. (9) and (11) the gas volumetric flux $\bar{\varepsilon}_G \bar{w}_G$ is constant and given by $J_{G,0}$. The volume fraction $\bar{\varepsilon}_G$ is thus calculated from $\bar{w}_G$ as

$$\bar{\varepsilon}_G = \frac{J_{G,0}}{\bar{w}_G}. \tag{12}$$

Some profiles of $\bar{\varepsilon}_G$ are shown in Fig. 1(b)(ii). As expected from Eq. (12) and from the $\bar{w}_G$ profiles in Fig. 1(b)(i), a sublayer rich in bubbles is formed on the bottom wall. As $\bar{w}_G$ increases from $W_{G,0}$ to V_∞, the volume fraction decreases from $J_{G,0}/W_{G,0}$ to a smaller value $J_{G,0}/V_\infty$ in the sublayer. The stratification in the mean density of liquid-gas mixture is potentially unstable to the gravity inside the sublayer.

C. Dimensionless governing equations

Adopting scales d of length, ν/d of velocity, d^2/ν of time, and $J_{G,0}d/\nu$ of bubble volume fraction, we nondimensionalize the governing equations (1)–(4) to obtain

$$\frac{\partial \varepsilon_G}{\partial t} + \boldsymbol{\nabla} \cdot (\varepsilon_G \mathbf{u}_G) = 0, \tag{13}$$

$$\frac{D\mathbf{u}_G}{Dt} = 3\frac{D\mathbf{u}}{Dt} - \frac{18}{r_b^2}(\mathbf{u}_G - \mathbf{u})$$
$$- (\mathbf{u}_G - \mathbf{u}) \times (\boldsymbol{\nabla} \times \mathbf{u}) + \frac{18}{\text{Pr} \cdot r_b^2}\mathbf{e}_z, \tag{14}$$

$$\boldsymbol{\nabla} \cdot \mathbf{u} = 0, \tag{15}$$

$$\frac{D\mathbf{u}}{Dt} = -\boldsymbol{\nabla}p + \Delta\mathbf{u} - \frac{9}{\text{Pr} \cdot r_b^2}\mathbf{e}_z$$
$$+ \varepsilon_G \frac{\text{Ra} \cdot r_b^2}{9\text{Pr}}\left(\frac{D\mathbf{u}}{Dt} + \frac{9}{\text{Pr} \cdot r_b^2}\mathbf{e}_z\right). \tag{16}$$

The boundary conditions (6) and (7) read in dimensionless form

$$\frac{\partial u}{\partial z} + \frac{\partial w}{\partial x} = 0, \quad w = 0, \quad \text{at } z = 1, \tag{17}$$

$$\mathbf{u} = 0, \quad w_G = w_{G,0}, \quad \varepsilon_G w_{G,0} = 1, \quad \text{at } z = -1. \tag{18}$$

We have introduced the following four dimensionless parameters:

$$\text{Pr} = \frac{\nu}{V_\infty d} = \frac{9\nu^2}{gR_b^2 d}, \quad \text{Ra} = \frac{gd^2 J_{G,0}}{V_\infty^2 \nu} = \frac{81\nu d^2 J_{G,0}}{gR_b^4},$$

$$w_{G,0} = \frac{W_{G,0}\, d}{\nu}, \quad r_b = \frac{R_b}{d}. \tag{19}$$

The first two parameters are Prandtl and Rayleigh numbers. They compare characteristic timescales: $\text{Pr} = T_R/T_\nu$ and $\text{Ra} = T_\nu T_R/T_B^2$, where T_R is the bubble residence time $T_R = d/V_\infty$, T_ν is the momentum diffusion time $T_\nu = d^2/\nu$, and T_B is the buoyancy time $T_B = \sqrt{d/g_r}$ with a reduced gravity $g_r = (J_{G,0}/V_\infty)\, g$. IK07 [16] and CM99 [17] employ Pr and

Ra similar to Eqs. (19) in their numerical investigations on bubbly convection flows. Throughout the present work, the injection velocity $w_{G,0}$ and bubble radius r_b are assumed to be $w_{G,0} = 1000$ and $r_b = 0.01$. Some results for other values of these parameters are given in Appendix B.

III. STABILITY ANALYSIS

We consider perturbations around the base state,

$$\mathbf{u} = \mathbf{u}', \quad \mathbf{u}_G = \bar{w}_G \mathbf{e}_z + \mathbf{u}'_G, \quad \varepsilon_G = \bar{\varepsilon}_G + \varepsilon'_G, \quad (20)$$

where perturbation components are indicated by primes and $\mathbf{u}' = u'\mathbf{e}_x + w'\mathbf{e}_z$, $\mathbf{u}'_G = u'_G\mathbf{e}_x + w'_G\mathbf{e}_z$ ($\mathbf{e}_x$: the unit vector in the x direction). Substituting Eqs. (20) into Eqs. (13)–(16) and linearizing the resulting equations with respect to perturbation fields, we have

$$\frac{\partial \varepsilon'_G}{\partial t} = -\left(\bar{w}_G \frac{\partial}{\partial z} + \frac{d\bar{w}_G}{dz} \right) \varepsilon'_G - \bar{\varepsilon}_G \frac{\partial u'_G}{\partial x}$$
$$- \left(\bar{\varepsilon}_G \frac{\partial}{\partial z} + \frac{d\bar{\varepsilon}_G}{dz} \right) w'_G, \quad (21)$$

$$\frac{\partial \mathbf{u}'_G}{\partial t} + \bar{w}_G \frac{\partial \mathbf{u}'_G}{\partial z} + \frac{d\bar{w}_G}{dz} w'_G \mathbf{e}_z$$
$$= 3\frac{\partial \mathbf{u}'}{\partial t} - \frac{18}{r_b^2}(\mathbf{u}'_G - \mathbf{u}') + \bar{w}_G \zeta' \mathbf{e}_x, \quad (22)$$

$$\nabla \cdot \mathbf{u}' = \mathbf{0}, \quad (23)$$

$$\frac{\partial \mathbf{u}'}{\partial t} = -\nabla \pi' + \Delta \mathbf{u}' + \bar{\varepsilon}_G \frac{\mathrm{Ra} \cdot r_b^2}{9\mathrm{Pr}} \frac{\partial \mathbf{u}'}{\partial t} + \varepsilon'_G \frac{\mathrm{Ra}}{\mathrm{Pr}^2} \mathbf{e}_z, \quad (24)$$

where ζ' is the liquid vorticity perturbation, $\zeta' = \partial_z u' - \partial_x w'$, and π' is the perturbation of a reduced pressure. The boundary conditions on the perturbation fields are obtained from Eqs. (17) and (18). They are

$$\frac{\partial u'}{\partial z} + \frac{\partial w'}{\partial x} = w' = 0, \quad \text{at } z = 1, \quad (25)$$

$$u' = w' = w'_G = \varepsilon'_G = 0, \quad \text{at } z = -1. \quad (26)$$

We perform a modal analysis to determine the stability of the base state, expanding the perturbation fields into normal modes:

$$(\mathbf{u}'_G, \mathbf{u}', \varepsilon'_G) = \int_{-\infty}^{\infty} (\hat{\mathbf{u}}_G, \hat{\mathbf{u}}, \hat{\varepsilon}_G) e^{st+ikx} \, dk, \quad (27)$$

where k is the wave number and $s = \sigma + i\omega$ is the complex growth rate consisting of a growth rate σ and a frequency ω. Hatted quantities are the complex amplitudes of perturbation fields.

For a mode of wave number k, Eqs. (21)–(26) can be cast into the following form:

$$\mathcal{A}(k, \mathrm{Pr}, \mathrm{Ra}, w_{G,0}, r_b) \hat{\mathbf{X}} = s\mathcal{B} \hat{\mathbf{X}}, \quad (28)$$

where $\hat{\mathbf{X}} = (\hat{\mathbf{u}}_G, \hat{\mathbf{u}}, \hat{\varepsilon}_G)^{tr}$. A linear differential operator $\mathcal{A}$ with respect to z depends on the wave number k and the parameters (Pr, Ra, $w_{G,0}$, r_b). The coefficient matrix $\mathcal{B}$ is constant. We discretize the eigenvalue problem (28) with the Lobatto-Gauss-collocation method based on Chebyshev series expansion and determine eigenvalues s by the QZ decomposition.

IV. RESULTS

A. Stability diagram

The growth rate σ of the least stable mode determined from the eigenvalue problem (28) changes its sign from negative to positive with increasing Rayleigh number Ra from zero at a given wave number k. Determining the marginal stability condition where the sign of σ changes for different wave numbers while keeping r_b and $w_{G,0}$ constant, we obtain the marginal stability curve $\sigma(k, \mathrm{Ra}) = 0$ [Fig. 2(a)]. The curve shifts downward with decreasing Prandtl number Pr changing its shape. It has only a single minimum point for Pr $> 4.13 \times 10^{-5}$, while there exist two local minima otherwise. At Pr $= 3.25 \times 10^{-5}$ (=: Pr*) the two minima are found at the same value of Ra $= 645$ (=: Ra*). Marginally stable modes are stationary except for a range of k found at small Pr (see the lowest curve in the figure).

Eigenvectors of some marginal modes are shown in Fig. 2(b) for the gas volume fraction ε'_G and liquid velocity $\mathbf{u}'$. The perturbation gas volume fraction ε'_G exhibits different structures consisting of horizontal arrays of bubble-rich and bubble-poor cells [Fig. 2(b)]. For stationary modes [Fig. 2(b) i–viii], the horizontal flow of the liquid phase converges and diverges in cells of large and small ε'_G, respectively. In the lowest layer attached to the bottom wall, where the unstable density stratification is the most significant, the liquid moves upward inside bubble-rich cells and downward inside bubble-poor cells. Convection rolls on the bottom do not extend to the top free surface of fluid layer for large k [Fig. 2(b) i–iii, v, vii]: multilayer convection rolls are observed, though the flow in convection rolls away from the bottom wall is much weaker than that in the rolls on the wall. For small k, in contrast, convection rolls on the wall occupy the entire fluid layer [Fig. 2(b) iv, vi, viii]. We call them whole-layer convection rolls. The gas velocity field $\mathbf{u}'_G$ exhibits the same flow patterns as the liquid velocity field $\mathbf{u}'$. The slip velocity $\mathbf{u}'_G - \mathbf{u}'$ is only on the order of a few percent of $\mathbf{u}'$. Pr determines the types of convection rolls, i.e., either multi- or whole-layer mode, at critical conditions. Oscillatory eigenmodes [Fig. 2(b) ix] are also composed of multilayer cells of gas volume fraction. The perturbation flow rises and falls in bubble-rich and bubble-poor cells attached to the bottom, respectively. In contrast to stationary modes, the structures of cells and flows of oscillatory modes lack $x \to -x$ reflection symmetry.

Variations of the critical parameters (k_c, Ra$_c$) determined from the marginal curves are shown in Fig. 3. The critical Rayleigh number Ra$_c$ increases with Pr, while the critical wave number k_c varies nonmonotonically. The behavior of (k_c, Ra$_c$) for Pr $<$ Pr* is distinct from the behavior for Pr $>$ Pr*, since whole-layer and multilayer modes are critical in the former and latter cases, respectively. At the codimension-two point Pr $=$ Pr*, both types of modes are critical.

Whole-layer convection rolls were observed in the numerical simulation by CM99 [17]. These authors reported convection rolls of different geometrical characteristics for the same set of parameter values (Pr, Ra, r_b) = (2.5 × 10^{-4}, 2.07 × 10^5, 2 × 10^{-3}). The aspect ratio Γ of the wavelength of observed convection pattern to the fluid layer thickness is either 1 or 0.5. For this Prandtl number and bubble
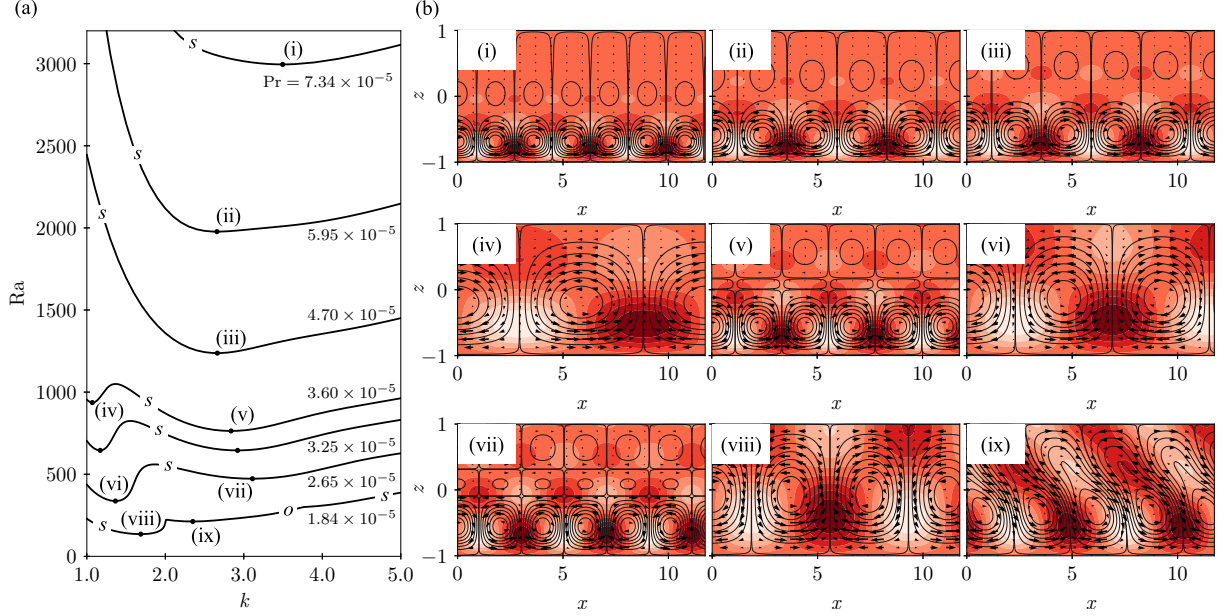
FIG. 2. (a) Marginal stability curves, above which the quiescent state is unstable, for different values of the Prandtl number Pr in the k-Ra space. The gas injection velocity and the bubble radius are fixed at $w_{G,0} = 1000$ and $r_b = 0.01$. The temporal natures of marginally stable mode are indicated on curves by s (stationary) and o (oscillatory). (b) Eigenvectors at the local minimum points (i)–(ix). The liquid velocity $\mathbf{u}' = (u', w')$ and the gas fraction ε'_G are shown by vectors and colors, respectively. Bubble-rich and bubble-poor cells correspond to red and white zones. Some streamlines are also shown in (b) to visualize the structures of liquid flows.

radius, the present linear stability analysis does not predict any instability.

Experiments on a RT-like instability of bubble layers by IK07 [16] showed the formation of whole-layer convection rolls at $Pr = O(10^{-2})$, $Ra = O(10^5)$, and $r_b = O(10^{-3})$. The numerical simulations performed by these authors showed also the formation of whole-layer convection for experimental values of Pr and Ra. The ratio Γ was found to increase with Ra and to take a value 2.7 close to the onset of convection formation. For the critical modes reported in Fig. 3, the ratio Γ ($= \pi/k_c$) is smaller than 1.3 for multilayer mode and between 1.5 and 3.1 for whole-layer mode. Bubbly convection observed by IK07 [16] might correspond to whole-layer modes in the present work. The present linear stability theory
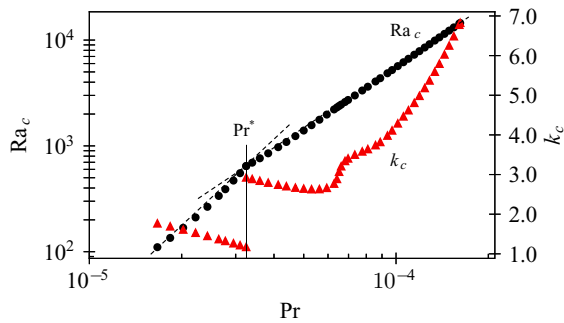
predicts, however, no instability at Ra $\sim 10^5$ for the values of (Pr, r_b) considered in IK07 [16]. In fact, for tiny bubbles in a viscous liquid such as considered in IK07 [16], the base state (8) has a uniform bubble distribution throughout the fluid layer, $\bar{\varepsilon}_G = $ const, so that the density stratification is stable to gravity. The instability investigated by IK07 [16] would be related to a particular initial configuration, i.e., an unstable superposition of a pure liquid layer over a bubble layer, and would be distinct from the instability considered in the present work.

B. Energy budget analysis

We consider the energy transfer from the base to perturbation flows in order to obtain insights into the instability mechanism. The transfer to liquid perturbation flows will be similar to that in RB convection because of the similarity of Eqs. (23) and (24) with the corresponding equations for thermal convection [30]. The perturbation flows gain and lose energy due to buoyancy and viscous energy dissipation, respectively. To confirm this scenario we can derive an evolution equation for the kinetic energy of liquid flows by taking the inner product of Eq. (24) with $\mathbf{u}'$. After integrating the resulting equation over the whole liquid layer and averaging it with respect to the horizontal direction, we obtain

$$\frac{dK}{dt} = W_B - D_V, \qquad (29)$$

where the kinetic energy K, the power of the buoyancy force W_B, and the rate of viscous energy dissipation D_V are

FIG. 3. Variation of critical parameters (k_c, Ra$_c$) as function of Pr. The whole- and multilayer modes are critical on the left and right of a codimension-two point Pr = Pr*, respectively. The best-fitting power laws Ra$_c \propto$ Pr^n are shown in dashed lines. The exponent n is 2.68 and 1.93 for the left and right lines.
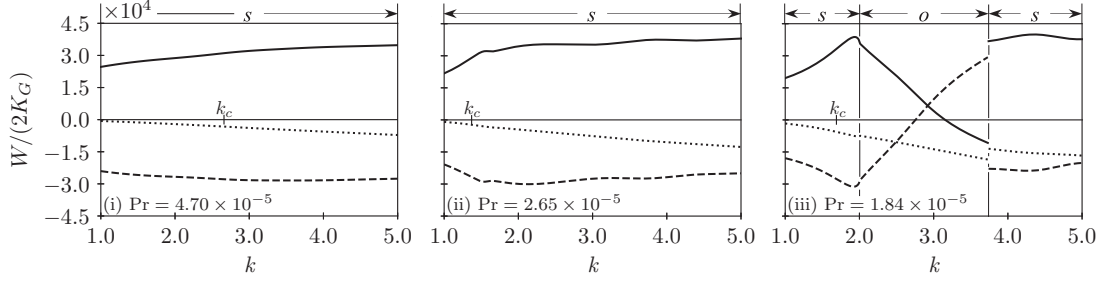
FIG. 4. Powers providing energy to perturbation gas flows at marginally stable conditions: W_I (solid line), W_D (dotted line), and W_L (dashed line) represent the powers of liquid inertia and drag and lift forces, respectively. The powers have been normalized by twice the kinetic energy K_G of perturbation flows. Different panels show results for different values of the Prandtl number Pr. The values of critical wave number k_c are marked on the k axis. The temporal natures of marginally stable mode are indicated by s (stationary) and o (oscillatory) at the top of each panel.

defined by

$$K = \left\langle \left(1 - \bar{\varepsilon}_G \frac{\mathrm{Ra} \cdot r_b^2}{9\mathrm{Pr}}\right) \frac{u'^2 + w'^2}{2} \right\rangle, \tag{30}$$

$$W_B = \frac{\mathrm{Ra}}{\mathrm{Pr}^2} \langle \varepsilon_G' w' \rangle, \tag{31}$$

$$D_V = \langle \Phi \rangle, \tag{32}$$

where the dissipation function Φ is given as $\Phi = 2(\partial_x u')^2 + (\partial_z u' + \partial_x w')^2 + 2(\partial_z w')^2$ and the angle brackets denote the following integral operation:

$$\langle \bullet \rangle = \frac{k}{2\pi} \int_{-1}^{1} \int_{0}^{2\pi/k} \bullet \, dx \, dz. \tag{33}$$

Equation (29) confirms that convection develops when the buoyancy overcomes the viscous energy dissipation.

We should now turn to the energy transfer in gas phase, as the driving buoyancy effect W_B is created by a heterogeneous distribution of the gas phase due to perturbation gas flows. By similar procedures used to obtain Eq. (29), we derive the following evolution equation from Eq. (22).

$$\frac{dK_G}{dt} = W_I + W_D + W_L, \tag{34}$$

where the kinetic energy K_G and the powers of the liquid inertia W_I, of the drag W_D, and of the lift W_L are defined by

$$K_G = \left\langle \frac{u_G'^2 + w_G'^2}{2} \right\rangle, \tag{35}$$

$$W_I = -\left\langle \bar{w}_G \frac{\partial}{\partial z} \frac{\|\mathbf{u}_G'\|^2}{2} + \frac{d\bar{w}_G}{dz} w_G'^2 \right\rangle + 3\left\langle \frac{\partial \mathbf{u}'}{\partial t} \cdot \mathbf{u}_G' \right\rangle, \tag{36}$$

$$W_D = -\frac{18}{r_b^2} \langle (\mathbf{u}_G' - \mathbf{u}') \cdot \mathbf{u}_G' \rangle, \tag{37}$$

$$W_L = \langle \bar{w}_G \zeta' u_G' \rangle. \tag{38}$$

Energy budgets of the gas flow are computed for marginal modes for different values of Pr (Fig. 4). For stationary modes, the liquid inertia provides energy to perturbation flows (i.e., $W_I > 0$) regardless of the type of convection roll, while the drag and lift have stabilizing effects (i.e., $W_D, W_L < 0$). The liquid inertia and the lift become stabilizing and destabilizing for some oscillatory modes, e.g., when Pr $= 1.84 \times 10^{-5}$ for wave numbers k between 2.9 and 3.8.

V. DISCUSSION

The results for the critical parameters presented in Sec. IV are in marked contrast with the observations for the RT-like instability by CM99 [17]. These authors observed the formation of whole-layer convection of different aspect ratios ($\Gamma = 1$ and 0.5) for the same set of parameter values (Pr, Ra) $= (2.5 \times 10^{-4}, 2.07 \times 10^5)$ and suggested the absence of wave number selection. The present results (Fig. 2) show, in contrast, that a unique mode, *either* a multilayer mode ($\Gamma \leqslant 1.3$) *or* a whole-layer mode ($\Gamma = 1.5$–3.1), is selected depending on Pr. Like the present work, CM99 assumes no hydrodynamic diffusion and is based on the same governing equations as Eqs. (1)–(4) except for the Lagrangian approach to the bubble dynamics. The absence of wave number selection would hence not be related to the absence of hydrodynamic diffusion. Our analysis showed that the selection mechanism exists even in the absence of bubble-bubble interactions. Different convection patterns observed in CM99 would thus indicate the multistability of the bubbly flow system rather than the absence of wave number selection. Different attractors would be present under a given flow condition. A nonlinear bifurcation analysis and a stability analysis of secondary flows could elucidate this point.

As the energy budget equation (29) shows, the instability of bubbly flows found in Sec. IV is provoked by the buoyancy. More buoyant lower fluid overturns less buoyant upper fluid, once the buoyancy overcomes the stabilization by the viscous force. This principal mechanism is similar to that of thermal instabilities. There exist, however, essential differences between these instabilities in the transport of buoyancy sources. In thermal convection, the heat diffusion tends to homogenize temperature fields to produce stabilizing effects. In bubble convection, in contrast, stabilization arises from the transport of bubbles by the lift forces as shown by the energy budget analysis in Sec. IV B. In fact, the lift force $\bar{w}_G \zeta' \mathbf{e}_x$ in the gas momentum equation (22) is directed from bubble-rich to bubble-poor cells on the wall [see Fig. 2(b), noting that $\zeta' > 0$ and < 0 inside clockwise and counterclockwise convection rolls, respectively]. Thus, the lift force tends to homogenize the bubble distribution in the bottom layer of fluid where the buoyancy drives convection [31]. Stabilizing effects of lift force are also reported in the literature on bubble columns [32].

The transport of buoyancy sources in bubble convection can give rise to multilayer convection rolls, even though the mean density increases monotonically in the base state [Fig. 1(a)]. Multilayer convection rolls are observed in double diffusive systems and have been investigated in geophysical and astrophysical contexts. For example, a variety of convection patterns can be produced in the Earth's mantle depending on the competition between destabilizing thermal density anomaly and stabilizing chemical density anomaly [33]. When the former effect predominates the latter one, whole-layer convection rolls develop. Otherwise, multilayer convection rolls emerge [34,35]. In ordinary thermal convection, superposed convection rolls can be observed in particular configurations, e.g., above a localized heat source in a stably stratified fluid layer [36], where the thermal stratification is unstable to gravity only slightly above the heat source. Otherwise, multilayer structures are rarely formed even for nonlinear temperature profiles due to internal heating [37]. In the present two-phase system, critical multilayer modes are observed for small Pr. The formation of multilayer convection could be explained from the perturbation in bubble distribution. In contrast to the ordinary thermal convection, the cells of buoyancy sources, i.e., the cells of positive ε'_G [see Fig. 2(b)] attached on the bottom wall extend only up to half the height of convection rolls. Above each of these cells, there is a cell of negative buoyancy sources, i.e., cells of negative ε'_G, in which the upward motion of convective flow is impeded by a net downward force resulting from a small number of bubbles. This implies a stabilizing effect at the upper part of convection rolls as in double diffusive systems exhibiting multilayer convection rolls.

VI. SUMMARY

In the present paper, we have revisited the problem of homogeneous-heterogeneous regime transition by performing a linear stability analysis for ascending bubbles in a quiescent liquid layer. We determined marginal stability curves Ra = Ra(k) for different values of Pr. While the curves have single minima for $Pr > 4.13 \times 10^{-5}$, there exist multiple minima otherwise. The marginal modes are stationary except for limited ranges of wave number at small Pr. Critical conditions (k_c, Ra_c) for $Pr < Pr^* = 3.25 \times 10^{-5}$ are distinct from those for $Pr > Pr^*$. In the former and latter cases, the critical modes consist of whole-layer and multilayer convection rolls, respectively. At a condimension two point $(Pr, Ra) = (Pr^*, Ra^*)$, both multi- and whole-layer modes are critical. These results show that the mechanism of wave number selection exists even in the absence of bubble-bubble interactions. Different convection patterns observed in CM99 [17] indicate the multistability of the bubbly flow system. A nonlinear bifurcation analysis could elucidate the presence of different attractors and their stability.

We have also examined the energy transfer from the base to perturbation flows in order to understand the instability mechanism. Liquid perturbation flows gain and lose energy due to buoyancy and viscous dissipation, respectively. The driving buoyancy is created by a heterogeneous distribution of bubbles. For critical modes, gas perturbation flows, which generate this nonequilibrated bubble distribution, gain energy

from the inertial forces on bubbles. The lift forces on bubbles tend, in contrast, to damp the gas flows through homogenization of the bubble distribution close to the wall. The drag forces are also found to have stabilizing effects.

APPENDIX A: EFFECTS OF DRAG COEFFICIENT MODEL

The model of drag coefficient affects the stability of the bubbly flow system, as the inverse density profile in the base state is different between models. In addition to the stability analysis obtained with $C_D = 48/Re_b$, we have performed similar analyses with different models of drag coefficient: $C_D = 16/Re_b$ [38,39] for bubbles in a pure liquid in the low Reynolds number limit, $C_D = 24/Re_b$ [40] for bubbles in a liquid contaminated by surfactants also in the low Reynolds number limit, and $C_D = (24/Re_b)\{2/3 + [12/Re_b + 0.75(1 + 3.315/\sqrt{Re_b})]^{-1}\}$ [41] which interpolates smoothly C_D for bubbles in a pure liquid from the low Reynolds number limit ($C_D = 16/Re_b$) to the large Reynolds number limit ($C_D = 48/Re_b$). Marginal stability conditions are quantitatively different between models. For models giving larger drags (i.e., for models with a larger value of $C_D Re_b$), the inverse density profile is confined in a thinner sublayer of fluid on the bottom wall and the critical value of Ra becomes larger. The analyses predict, however, the qualitatively same behavior of the bubbly flow system as that reported in the main text. In all the analyses, multi- and whole-layer critical modes are observed, and the transition between these two modes is predicted with varying Pr (Fig. 5).
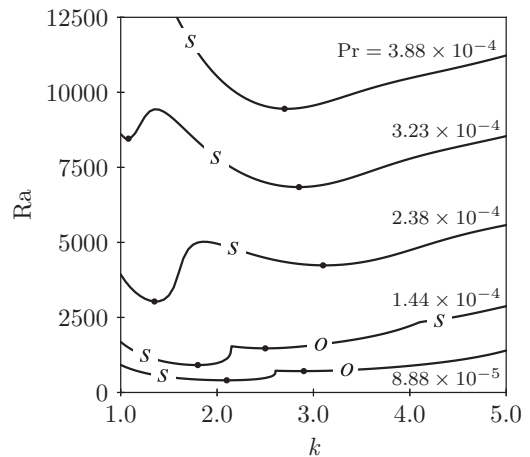

FIG. 5. Marginal stability curves, above which the quiescent state is unstable, for different values of Prandtl number Pr in the k-Ra space. The bubble radius and the bubble injection velocity are fixed at $r_b = 0.01$ and $w_{G,0} = 1000$. The drag coefficient is modeled by $C_D = 16/Re_b$ [38,39].

APPENDIX B: EFFECTS OF THE BUBBLE RADIUS r_b AND THE INJECTION VELOCITY $w_{G,0}$

The value of the r_b affects the stability of the bubbly flow layer significantly, as the inverse density profile in the base state is sensitive to r_b. For example, the critical value of Ra is $Ra_c = 73.96$ for $r_b = 0.014$ and $Ra_c = 2997$ for $r_b = 0.006$ (Fig. 6). These values are, respectively, 0.22 times smaller and 8.91 times larger than the critical Ra for $r_b = 0.01$. However, the predicted behavior of the bubbly flow system is qualitatively the same as that reported in the main text. Multi- and whole-layer critical modes are observed, and the transition between these two flow patterns is predicted with varying Pr.

The inverse density profile of the base state changes only slightly with varying the injection velocity $w_{G,0}$. As a consequence, the variation of $w_{G,0}$ does not affect the stability, unless $w_{G,0}$ is very close to the dimensionless terminal rising velocity $v_\infty = V_\infty/v/d$. For example, no qualitative and quantitative difference is produced by a variation of $w_{G,0}$ in a range $0 < w_{G,0}/v_\infty < 0.15$ for $Pr = 2.65 \times 10^{-5}$.
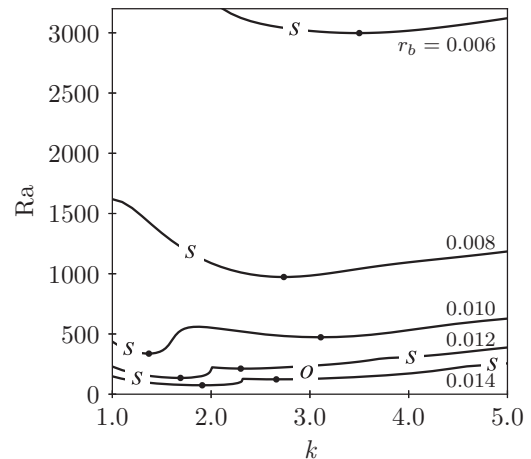

FIG. 6. Marginal stability curves for different values of bubble radius r_b in the k-Ra space. Prandtl number Pr and the injection velocity are fixed at $Pr = 2.65 \times 10^{-5}$ and $w_{G,0} = 1000$. The temporal natures of marginally stable mode are indicated on curves by s (stationary) and o (oscillatory).

[1] D. Lohse, Bubble puzzles: From fundamentals to applications, Phys. Rev. Fluids **3**, 110504 (2018).

[2] S. L. Ceccio, Friction drag reduction of external flows with bubble and gas injection, Annu. Rev. Fluid Mech. **42**, 183 (2010).

[3] Y. Murai, Frictional drag reduction by bubble injection, Exp. Fluids **55**, 1773 (2014).

[4] B. Dollet, P. Marmottant, and V. Garbin, Bubble dynamics in soft and biological matter, Annu. Rev. Fluid Mech. **51**, 331 (2010).

[5] K. Ferrara, R. Pollard, and M. Borden, Ultrasound microbubble contrast agents: Fundamentals and application to gene and drug delivery, Annu. Rev. Biomed. Eng. **9**, 415 (2007).

[6] F. Risso, Agitation, mixing, and transfers induced by bubbles, Annu. Rev. Fluid Mech. **50**, 25 (2018).

[7] R. F. Mudde, Gravity-driven bubbly flows, Annu. Rev. Fluid Mech. **37**, 393 (2005).

[8] W. K. Harteveld, R. F. Mudde, and E. Akker, Dynamics of bubble column: Influence of gas distribution on coherent structures, Can. J. Chem. Eng. **81**, 389 (2003).

[9] W. K. Harteveld, Bubble column: Structures and stability? Ph.D. thesis, Delft University of Technology, Delft, the Netherlands, 2005.

[10] D. Colombet, D. Legendre, F. Risso, A. Cockx, and P. Guiraud, Dynamics and mass transfer of rising bubble in a homogeneous swarm at large gas volume fraction, J. Fluid Mech. **763**, 254 (2015).

[11] M. C. Ruzicka, On stability of a bubble column, Chem. Eng. Res. Des. **91**, 191 (2013).

[12] A. I. Shnip, R. V. Kolhatkar, D. Swamy, and J. B. Joshi, Criteria for the transition from the homogeneous to the heterogeneous regime in two dimensional bubble column reactors, Int. J. Multiphase Flow **18**, 705 (1992).

[13] S. M. Monahan and R. O. Fox, Linear stability analysis of a two-fluid model for air-water bubble columns, Chem. Eng. Sci. **62**, 3159 (2007).

[14] S. M. Monahan and R. O. Fox, Validation of two-fluid simulations of a pseudo-two-dimensional bubble column with uniform and nonuniform aeration, Ind. Eng. Chem. Res. **48**, 8134 (2009).

[15] R. Kimura, Cell formation in the convective mixed layer, Fluid Dyn. Res. **3**, 395 (1988).

[16] K. Iga and R. Kimura, Convection driven by collective buoyancy of microbubbles, Fluid Dyn. Res. **39**, 68 (2007).

[17] E. Climent and J. Magnaudet, Large-Scale Simulations of Bubble-Induced Convection in a Liquid Layer, Phys. Rev. Lett. **82**, 4827 (1999).

[18] M. C. Ruzicka and N. H. Thomas, Buoyancy-driven instability of bubbly layers: Analogy with thermal convection, Int. J. Multiphase Flow **29**, 249 (2003).

[19] G. Kong, H. Mirsandi, K. A. Buist, E. J. A. F. Peters, M. W. Baltussen, and J. A. M. Kuipers, Hydrodynamic interaction of bubbles rising side-by-side in viscous liquids, Exp. Fluids **60**, 155 (2019).

[20] M. C. Ruzicka, J. Zahradnik, J. Drahos, and N. H. Thomas, Homogeneous–heterogeneous regime transition in bubble columns, Chem. Eng. Sci. **56**, 4609 (2001).

[21] J. R. Grace, T. Wairegi, and T. H. Nguyen, Shapes and velocities of single drops and bubbles moving freely through immiscible liquids, Trans. Inst. Chem. Eng. **54**, 167 (1976).

[22] M. K. Tripathi, K. C. Sahu, and R. Govindarajan, Dynamics of an initially spherical bubble rising in quiescent liquid, Nat. Commun. **6**, 6268 (2015).

[23] J. Magnaudet and I. Eames, The motion of high-Reynolds-number bubbles in inhomogeneous flows, Annu. Rev. Fluid Mech. **32**, 659 (2000).

[24] V. G. Levich, *Physicochemical Hydrodynamics* (Prentice-Hall, NJ, 1962).

[25] O. A. Druzhinin and S. Elghobashi, Direct numerical simulation of bubble-laden turbulent flows using the two fluid formulation, Phys. Fluids **10**, 685 (1998).

[26] M. R. Maxey, E. J. Chang, and L. P. Wang, Simulation of interactions between microbubbles and turbulent flows, Appl. Mech. Rev. **47**, 70 (1994).

[27] P. M. Rightley and J. C. Lasheras, Bubble dispersion and interphase coupling in a free-shear flow, J. Fluid Mech. **412**, 21 (2000).

[28] I. M. Mazzitelli, D. Lohse, and F. Toschi, On the relevance of the lift force in bubbly turbulence, J. Fluid Mech. **488**, 283 (2003).

[29] P. Oresta, R. Verzicco, D. Lohse, and A. Prosperetti, Heat transfer mechanisms in bubbly Rayleigh-Bénard convection, Phys. Rev. E **80**, 026304 (2009).

[30] P. G. Drazin and W. H. Reid, *Hydrodynamic Stability* (Cambridge University Press, Cambridge, England, 2010).

[31] We have performed some linear stability analyses with $C_L = 0$ to confirm that the absence of the lift force leads to the formation of convection at smaller Ra than the critical values determined in Sec. IV.

[32] D. Lucas, H. M. Prasser, and A. Manera, Influence of the lift force on the stability of a bubble column, Chem. Eng. Sci. **60**, 3609 (2005).

[33] F. M. Richter and D. P. McKenzie, On some consequences and possible causes of layered mantle convection, J. Geophys. Res.: Solid Earth **86**, 6133 (1981).

[34] M. L. Bars and A. Davaille, Stability of thermal convection in two superimposed miscible viscous fluids, J. Fluid Mech. **471**, 339 (2002).

[35] A. Davaille, M. L. Bars, and C. Carbonne, Thermal convection in a heterogeneous mantle, C. R. Geosci. **335**, 141 (2003).

[36] K. E. Torrance, Natural convection in thermally stratified enclosures with localized heating from below, J. Fluid Mech. **95**, 477 (1979).

[37] Y. Tasaka and Y. Takeda, Effects of heat source distribution on natural convection induced by internal heating, Int. J. Heat Mass Transf. **48**, 1164 (2005).

[38] J. Hadamard, Mouvement permanent lent d'une sphère liquid et visqueuse dans un liquide visqueux, C. R. Acad. Sci. Paris **152**, 1735 (1911).

[39] W. Rybczynski, Uber die fortschreitende Bewegung einer flüssigen Kugel in einem zähen Medium, Bull. Acad. Sci. Cracovie A **1**, 40 (1911).

[40] G. G. Stokes, On the effect of the internal friction of fluids on the motion of pendulums, Trans. Cambridge Philos. Soc. **9**, 8 (1851).

[41] R. Mei, J. F. Klausner, and C. J. Lawrence, A note on the history force on a spherical bubble at finite Reynolds number, Phys. Fluids **6**, 418 (1994).